

Magnetic and thermodynamic substantiation of the efficiency of three-component $\text{Ho}_{1-x}\text{Er}_x\text{Ni}_2$ ($x = 0.25, 0.5, 0.75$) Laves-phases

Jacek Ćwik (✉ j.cwik@intibs.pl)

Institute of Low Temperature and Structure Research, PAS, Okólna 2, 50-422 Wrocław

Jurii Koshkidko

Institute of Low Temperature and Structure Research, PAS, Okólna 2, 50-422 Wrocław

Konstantin Nenkov

Leibniz IFW Dresden, Institute for Complex Materials, D-01069, Dresden

Evgenia Tereshina-Chitrova

Institute of Physics CAS, Prague 18221

Małgorzata Małecka

Institute of Low Temperature and Structure Research, PAS, Okólna 2, 50-422 Wrocław

Bruno Weise

Leibniz IFW Dresden, Institute for Complex Materials, D-01069, Dresden

Karolina Kowalska

Faculty of Chemistry, Wrocław University of Science and Technology, Norwida 4/6, 50-373 Wrocław

Article

Keywords:

Posted Date: April 20th, 2022

DOI: <https://doi.org/10.21203/rs.3.rs-1561990/v1>

License:   This work is licensed under a Creative Commons Attribution 4.0 International License.

[Read Full License](#)

Abstract

A wide variety of intriguing and exciting effects observed in solids results from the coupling of their magnetic sublattice with an applied magnetic field. In particular, it concerns the magneto-thermodynamic phenomenon well-known as the magnetocaloric effect (MCE), which manifests itself in the absorption and emission of heat by a solid under an external magnetic field change.

To date, significant efforts have been put into searching for materials with advanced magnetocaloric properties, which show promise as refrigerants that might ensure the reliable and efficient cooling technology being alternative to the conventional gas-compression-based technology. To fulfill the expectations, new compounds with improved and tailored MCE characteristics are designed and efficient procedures for their manufacturing are developed.

A great deal of attention has been paid to searching for magnetic refrigerants in view of industrial applications. Systems showing large MCEs at low temperatures are of importance due to their potential utilization in refrigeration for gas liquefaction.

We find that the Laves-phase rare-earth-nickel solid solutions give the possibility of reaching high magnetocaloric potentials in a wide temperature range, which is demonstrated by an example of the $\text{Ho}_{1-x}\text{Er}_x\text{Ni}_2$ compositions used as components of magnetocaloric composites.

Introduction

Magnetic refrigeration based on the magnetocaloric effect is an attractive approach to cooling technology, and is energy-efficient and eco-friendly as compared to conventional cooling methods [1–3]. The MCE is intrinsic to all magnetic materials; the phenomenon is due to the coupling of magnetic sublattice of a solid with an applied magnetic field, which changes the magnetic part of entropy of the solid. Like the gas compression, isothermal magnetization reduces entropy of magnetic material, which subsequently can be cooled by adiabatic demagnetization. In a reversible process, demagnetizing restores zero-field magnetic entropy of a system. Generally, MCE is defined by the isothermal magnetic entropy change, ΔS_{mag} , in an isothermal process and by the temperature change, ΔT_{ad} , in an adiabatic process. The values of the above magnetocaloric potentials usually are highest in the vicinity of a magnetic ordering temperature and decrease smoothly to zero beyond the magnetic phase transition region. The other correlated parameters that allow one to determine the magnetocaloric performance of magnetic material are the refrigerant capacity (RC) and relative cooling power (RCP) or temperature averaged entropy change (TEC) [4].

The search for new materials for cryogenics among RNi_2 (R – is a rare-earth metal) compositions, has its base in their structural, magnetic, and thermodynamic properties. Magnetocaloric cooling with rare-earth based Laves-phase materials offers higher efficiency for liquifying gases compared to conventional methods, e.g. hydrogen which is of great interest as an energy carrier in the decarbonization of the economy.

The RNi_2 compounds belong to the Laves phases and crystallize with the formation of a simple regular $MgCu_2$ -type structure (C15); appearance of a stable superstructure, based on the above structure and formed by regular vacancies at the rare-earth sites, is possible [5–8]. These compounds are characterized by high localized magnetic moments originating from the incompletely filled $4f$ -electron shell of lanthanides. The non-magnetic state of Ni atoms in these compounds is the cause of low magnetic ordering temperatures because the range of wave functions derived from lanthanides is lower than the interatomic distances, and $4f$ - $4f$ interactions are weak. The majority of RNi_2 compounds are found to be ferromagnetically ordered at low-temperatures and, upon ordering, exhibit the second-order magnetic phase transition [6, 9]. These features of RNi_2 compounds determine the marked MCE and, hence, their promise as cryogenic refrigeration materials.

The above considerations determine the possibility to make a “table-like” temperature dependence – $\Delta S_{mag}(T)$, namely, to reach the almost unchanged significant value of $-\Delta S_{mag}$ over a wide temperature range. In particular, it can be done with the $Ho_{1-x}Er_xNi_2$ compositions, for which the Curie temperatures (T_C) range between 13.5 and 6.5 K for $HoNi_2$ and $ErNi_2$ [10], respectively. It should be noted that the “table-like” behavior of $-\Delta S_{mag}(T)$ is the essential requisite for an ideal Ericsson-like refrigeration cycle [11].

The purpose of this work is to characterize the structure and magneto-thermodynamic properties of $Ho_{1-x}Er_xNi_2$ and to analyze their evolution in accordance with the substitutions in the rare-earth sublattice. We focus on the practical magnetocaloric aspect of the $Ho_{1-x}Er_xNi_2$ solid solutions. Direct and indirect measurements of magnetocaloric potentials in a wide magnetic-field range allow us to extend the knowledge on the magnetocaloric nature of considered compositions with the magnetic dilution determining their properties as composite refrigerant components.

Results

Structural analysis

The XRD patterns recorded for the $Ho_{1-x}Er_xNi_2$ solid solutions at room temperature were analyzed by the Rietveld method and are depicted in Fig. 1. Through the substitution of erbium for holmium in $Ho_{0.5}Er_{0.5}Ni_2$ and $Ho_{0.25}Er_{0.75}Ni_2$, the ordering of R vacancies preserved in the structure of $HoNi_2$ phase takes place, and the $2a$ cubic superstructure (space group $Fd\bar{3}m$) forms, indicated by indexed peaks marked with S in Figs. 1(a), 1(b). For the $Ho_{0.75}Er_{0.25}Ni_2$ stoichiometric composition, in contrast to $Ho_{0.5}Er_{0.5}Ni_2$ and $Ho_{0.25}Er_{0.75}Ni_2$, this effect is not so evident, reflections of the superstructure do not appear in the X-ray diffraction pattern, and the structure can be described by the space group $Fd\bar{3}m$.

According to Delsante et al. [5], formation of the regular C15 structure (space group $Fd\bar{3}m$) is expected for the RNi_2 compounds with the enthalpy of formation $\Delta_f H^\circ$ at 300 K of less than 40 kJ/mol. The enthalpies of formation $\Delta_f H^\circ$ of $HoNi_2$ and $ErNi_2$ equal to -48 and -50 kJ/mol, respectively, suggest the

emergence of the regular C15 structure in these compounds, which was indeed confirmed in our earlier work [10]. However, in the case of $\text{Ho}_{0.5}\text{Er}_{0.5}\text{Ni}_2$ and $\text{Ho}_{0.25}\text{Er}_{0.75}\text{Ni}_2$ solid solutions, this rule is not confirmed. Additional vacancies are induced and are responsible for the formation of the superstructure. Vacancies arise as structural defects resulting from differences in the atomic radii of elements comprising a solid solution. Owing to the difference in the atomic radii, Ho - Ni and Er - Ni bonds in the solid solutions differ in length; this fact has a direct impact on the formation of vacancies. Similar results were obtained for the Tb distribution in $\text{Tb}_{1-x}\text{Ho}_x\text{Ni}_2$ solid solutions [12] and are in line with the data obtained for the other ternary Laves-phase solid solutions, e.g., $\text{Tb}_{1-x}\text{Dy}_x\text{Ni}_2$ [13] studied previously.

According to the data given in Fig. 1, small amounts of Ho_2O_3 and Er_2O_3 impurity phases are present in the $\text{Ho}_{0.5}\text{Er}_{0.5}\text{Ni}_2$ and $\text{Ho}_{0.25}\text{Er}_{0.75}\text{Ni}_2$ samples, the total content of which is not more than 3 wt. %. For $\text{Ho}_{0.75}\text{Er}_{0.25}\text{Ni}_2$, the lattice parameter is equal to 7.1462 Å. For the two consecutive substitutions, the lattice parameter decreases as the Er content increases to $x = 0.75$. This is due to the fact that, in accordance with the lanthanide contraction, the radius of Er atoms is lower than that of Ho. It should be noted that the parent compounds, similarly to the $\text{Ho}_{0.75}\text{Er}_{0.25}\text{Ni}_2$ compound, solidify with the formation of the cubic C15 crystal structure.

The typical SEM image and EDX studies of the characteristic microstructure of the polished section as representative of $\text{Ho}_{0.25}\text{Er}_{0.75}\text{Ni}_2$ are shown in Fig. 2. The EDX analysis performed for large areas of samples showed that their chemical compositions are consistent with the nominal ones. Similar results were also obtained for the other samples.

Evaluation Of Magnetocaloric Effect By Indirect Method

Figures 3(a)-(c) show the temperature dependences of the total heat capacity, $C_{\text{tot}}(T)$, of the $\text{Ho}_{1-x}\text{Er}_x\text{Ni}_2$ solid solutions in zero magnetic field. Filled symbols correspond to the experimental data, and open symbols correspond to the magnetic part of heat capacity, $C_{\text{mag}}(T)$, obtained after subtraction of the electron and phonon contribution, $C_{\text{el+ph}}(T)$, which was estimated by Debye function (solid lines in Figs. 3(a)-(c)) according to the equation:

$$C_{\text{el+ph}}(T) = \gamma T + 9NR \left(\frac{T}{\Theta_D} \right)^3 \int_0^{\Theta_D/T} \frac{x^4 e^x}{(e^x - 1)^2} dx$$

1

where the first term represents the electronic heat capacity; the second term corresponds to the phonon Debye contribution; $N=3$ is the number of atoms per formula unit; R is the universal gas constant; and $x \equiv \hbar\omega/k_B T$. In the temperature range 2–100 K, the best fit for all the studied samples, could be obtained by fixing the parameter $\gamma = 3.8 \text{ mJ/molK}^2$, while the Debye temperature of the $\text{Ho}_{1-x}\text{Er}_x\text{Ni}_2$

system, similarly to that of the $\text{Dy}_{1-x}\text{Er}_x\text{Ni}_2$ system [14], increases as the Er content increases. In the absence of magnetic field, the temperature dependence of the heat capacity shows a peak corresponding to magnetic phase transition typical of ferromagnetic compounds. The Curie temperatures T_C of the $\text{Ho}_{0.75}\text{Er}_{0.25}\text{Ni}_2$ (Fig. 3(a)), $\text{Ho}_{0.5}\text{Er}_{0.5}\text{Ni}_2$ (Fig. 3(b)), and $\text{Ho}_{0.25}\text{Er}_{0.75}\text{Ni}_2$ (Fig. 3(c)) compounds are 12.0, 9.7, and 7.7 K, respectively.

Insets in Fig. 3(a)-(c) show the heat capacity, as a function of temperature, measured in zero, 1- and 2-T magnetic fields. The feature observed for all of the studied compositions is the broadening of the $C_{\text{tot}}(T)$ peak and reduction of its height, which takes place with the increasing applied magnetic field.

The magnetic part of the entropy $S_{\text{mag}}(T)$ was calculated by integrating the dependence $C_{\text{mag}}(T)/T$ for each composition (Fig. 3(d)-(f)). The fact that the dependence of entropy exhibits a strong tendency to saturation, but the entropy does not approach the theoretical maximum value $S_{\text{max}} = R \ln(2J+1)$ (where J is the total angular momentum of a rare earth ion) at the Curie temperatures can be explained by peculiarities in the ground-state level splitting by the crystal electric field (CEF) when several CEF levels are separated from others by a substantial energy gap [15]. Similar behavior was observed for other pseudo-binary Laves-phase compounds [14, 16, 17]. According to the theoretical calculations, the maximum magnetic entropy should equal to 23.2–23.4 J/molK. In the case of the tested solid solutions, the maximum value of S_{mag} for $\text{Ho}_{0.75}\text{Er}_{0.25}\text{Ni}_2$ and $\text{Ho}_{0.5}\text{Er}_{0.5}\text{Ni}_2$ is 21.4 J/molK at 100 K and is 22.3 J/molK for $\text{Ho}_{0.25}\text{Er}_{0.75}\text{Ni}_2$. This means that almost the total magnetic entropy associated with the magnetic process is utilized.

The temperature behaviour of the magnetic entropy in 1- and 2-T magnetic fields shows that the applied magnetic field leads to the decrease in S_{mag} near T_C . In particular, the maximum value of S_{mag} for $\text{Ho}_{0.75}\text{Er}_{0.25}\text{Ni}_2$ near T_C decreases from 15.1 to 10.5 J/molK in the applied magnetic field. The temperature dependences of the isothermal magnetic entropy change $\Delta S_{\text{mag}}(T)$ calculated using the heat capacity data according to the procedure reported in [14] and caused by 1- and 2-T magnetic field change, are shown in insets in Figs. 3(d)-(f). For a magnetic field change of 0–2 T, the experimental maximum ΔS_{mag} in the case of the $\text{Ho}_{0.75}\text{Er}_{0.25}\text{Ni}_2$ compound reaches the highest value of 4.6 J/mol K (16.3 J/kg K) near 12.1 K and, as the Er content increases, becomes lower and equals to 3.9 J/mol K (13.7 J/kg K) for the $\text{Ho}_{0.25}\text{Er}_{0.75}\text{Ni}_2$ sample near 8 K. Figures 4(a)-(c) show dependences of the adiabatic temperature change, ΔT_{ad} , for $\text{Ho}_{1-x}\text{Er}_x\text{Ni}_2$ with $x = 0.25, 0.5, \text{ and } 0.75$, which were derived from the heat capacity data obtained in 1- and 2-T magnetic fields. As is seen, the increase in the applied magnetic field leads to an increase in the adiabatic temperature change near T_C . Both at 1- and 2-T magnetic field changes, the highest magnetocaloric effect was observed for $\text{Ho}_{0.75}\text{Er}_{0.25}\text{Ni}_2$. The maximum ΔT_{ad} for $\text{Ho}_{0.75}\text{Er}_{0.25}\text{Ni}_2$ reaches 2.8 K (4.9 K) at 12.0 K, and, with increasing Er content, the maximum peak value of ΔT_{ad} decreases to 2.2 K (3.9 K) for $\text{Ho}_{0.25}\text{Er}_{0.75}\text{Ni}_2$ at 7.7 K for a magnetic field change of 1 (2) T. Table 1 summarizes the data on the experimental isothermal magnetic entropy change $\Delta S_{\text{mag}}(T)$ and adiabatic

temperature change $\Delta T_{ad}(T)$ for low external magnetic field changes, which were estimated by the indirect method using the heat capacity data.

Table 1

Magnetocaloric properties for the selected binary RNi_2 compounds and for the investigated $Ho_{1-x}Er_xNi_2$ solid solutions estimated from heat capacity measurements for magnetic field changes of 1 and 2 T. T_C is the magnetic phase transition temperature; $-\Delta S_{mag}$ is the maximum magnetic entropy change; ΔT_{ad} is the maximum adiabatic temperature change; RC is the refrigerant capacity; RCP is the relative cooling power; and TEC is the temperature averaged entropy change.

Compound	T_C (K)	$-\Delta S_{mag}$ (J/kgK)		ΔT_{ad} (K)		RC/RCP (J/kg)		$TEC(3)/TEC(10)$ (J/kgK)	
		0-1 T	0-2 T	0-1 T	0-2 T	0-1 T	0-2 T	0-1 T	0-2 T
TbNi ₂ [23]	37.1	3.4	6.5	1.4	2.4	34/44	94/122	3.2/2.9	6.4/6.0
DyNi ₂ [23]	21.8	6.3	11.1	2.4	3.8	48/63	117/154	5.9/4.8	11.1/9.1
HoNi ₂ [10]	13.5	8.8	14.6	2.7	4.6	55/72	128/171	8.0/6.2	14.9/11.4
Ho _{0.75} Er _{0.25} Ni ₂	12.0	10.0	16.2	2.8	4.9	49/65	117/155	8.9/4.9	15.1/9.1
Ho _{0.5} Er _{0.5} Ni ₂	9.7	10.3	15.5	2.7	4.5	52/72	123/163	9.0/6.8	15.1/11.8
Ho _{0.25} Er _{0.75} Ni ₂	7.7	8.8	13.7	2.2	3.9	45/58	102/133	8.0/5.6	12.6/10.4
ErNi ₂ [10]	6.2	8.6	13.0	2.2	3.8	43/55	96/122	7.8/5.3	12.1/9.3
Composite 1	-	6.7	-	-	-	57/67	-	6.6/5.6	-
Composite 2	-	-	12.0	-	-	-	121/150	-	11.9/10.4

To compare the refrigeration properties of $Ho_{1-x}Er_xNi_2$ with those of the other previously investigated RNi_2 compounds, the refrigerant capacities (RC), relative cooling power (RCP) and temperature averaged entropy change (TEC) were estimated. The first parameter is a measure of the amount of heat that can be transferred between the cold and hot sinks in one ideal refrigeration cycle and were estimated by integrating the $\Delta S_{mag}(T)$ curve over the full width at half maximum [18, 19]. It should be noted that, as the magnetic entropy change decreases owing to the Er doping in $Ho_{1-x}Er_xNi_2$, the RC also reduces, but it is still high, namely, ~ 45 J/kg and ~ 102 J/kg for a field change of 1 and 2 T, respectively.

The second parameter is defined as $\Delta S_{mag}^{(max)} \times \delta T_{FWHM}$, where δT_{FWHM} denotes the full width temperature span of ΔS_{mag} vs. T curve at its half maximum [20]. As the Er content increases, the RCP values decrease from 65 J/kg for $Ho_{0.75}Er_{0.25}Ni_2$ to 58 J/kg for $Ho_{0.25}Er_{0.75}Ni_2$ at the 1-T magnetic field

change and from 155 J/kg for $\text{Ho}_{0.75}\text{Er}_{0.25}\text{Ni}_2$ to 133 J/kg for $\text{Ho}_{0.25}\text{Er}_{0.75}\text{Ni}_2$ at the 2-T magnetic field change. It should be noted that, in the case of the $\text{Ho}_{0.5}\text{Er}_{0.5}\text{Ni}_2$ solid solution, there are slight deviations for both the obtained RC and RCP values from the expected ones.

The third parameter, the temperature averaged entropy change (TEC), was introduced by Griffith et al. [21] and the magnitude is calculated by the following formula:

$$TEC(\Delta T_{\text{lift}}) = \frac{1}{\Delta T_{\text{lift}}} \max_{T_{\text{mid}}} \left(\int_{T_{\text{mid}} - \frac{\Delta T_{\text{lift}}}{2}}^{T_{\text{mid}} + \frac{\Delta T_{\text{lift}}}{2}} |\Delta S_M|(T) \mu_0 \Delta H, T dT \right)$$

2

where ΔT_{lift} is the desired lift of temperature and T_{mid} is the temperature of the center of the TEC and is determined by maximizing the TEC value. Accordingly, two different ΔT_{lift} values of 3 and 10 K are chosen to calculate TEC for the $\text{Ho}_{1-x}\text{Er}_x\text{Ni}_2$ solid solutions under study. The resulted values of TEC (3 K) and TEC (10 K) at $\mu_0 \Delta H = 1$ T oscillate between 8.0-9.4 and 4.9-6.8 J/kgK and, at $\mu_0 \Delta H = 2$ T, oscillate between 12.6-15.1 and 9.1-11.8 J/kgK, respectively.

The obtained values are of a high level and are comparable to those obtained for other promising low temperature magnetocaloric materials, such as TbNi_2 [22, 23] DyNi_2 [23, 24], ErNi_2 , HoNi_2 [10], $\text{Dy}_{1-x}\text{Er}_x\text{Ni}_2$ [14], $\text{Tb}_{1-x}\text{Ho}_x\text{Ni}_2$ [12], TmCoAl [25], ErRu_2Si_2 [26], or $\text{HoNi}_2\text{B}_2\text{C}$ [27].

Due to the fact that the ideal Ericsson cycle employs a constant value of ΔS_{mag} in the temperature range of refrigeration, which is necessary for improving regeneration processes, composite materials were considered. It is expected that a composite material formed by at least two magnetic $\text{Ho}_{1-x}\text{Er}_x\text{Ni}_2$ compounds differing in the Er concentration could exhibit a “table-like” behavior of MCE in a wider temperature range. In this context, according to a procedure proposed in Refs. [11, 28, 29], numerical simulations were done to construct a composite material formed by $\text{Ho}_{1-x}\text{Er}_x\text{Ni}_2$ compounds. The isothermal magnetic entropy change of a magnetic composite $\Delta S_{\text{mag}}^{\text{comp}}$ based on N kinds of magnetic materials is equal to the sum of their magnetic entropy changes $\Delta S_{\text{mag},j}$ weighted by a molar ratio y_j . In our case, for a magnetic field change of 0-1 T (composite 1), optimal molar ratios are $y_1 = 0.599$ for $\text{Ho}_{0.25}\text{Er}_{0.75}\text{Ni}_2$, $y_2 = 0.046$ for $\text{Ho}_{0.5}\text{Er}_{0.5}\text{Ni}_2$, and $y_3 = 0.355$ for $\text{Ho}_{0.75}\text{Er}_{0.25}\text{Ni}_2$, while, in the case of a magnetic field change of 0-2 T (composite 2), two compounds are sufficient with $y_1 = 0.706$ for $\text{Ho}_{0.25}\text{Er}_{0.75}\text{Ni}_2$ and $y_2 = 0.294$ for $\text{Ho}_{0.75}\text{Er}_{0.25}\text{Ni}_2$.

Figure 5 shows the calculated isothermal magnetic entropy changes for the composite based on $\text{Ho}_{1-x}\text{Er}_x\text{Ni}_2$ compounds, which are obtained for magnetic field changes of 1 and 2 T. It should be noted that,

both in 1- and 2-T magnetic field changes, the maximum magnetic entropy change of the composite material exhibits an almost constant value of $\Delta S_{\text{mag}}^{\text{comp}}$ that is around 6.7 J/kgK for $\mu_0\Delta H=1$ T and 12 J/kgK for $\mu_0\Delta H=2$ T. For both composites, calculated $\Delta S_{\text{mag}}^{\text{comp}}$ remains almost unchanged in a temperature range of 8 to 12 K. These results suggest that, in order to design the appropriate composition of a refrigerant, it is necessary to evaluate the corresponding optimal molar ratios using the value of external magnetic field change at which the refrigerator should operate. To compare the magnetocaloric performance of the proposed composites with that of their constituents, the values of RC , RCP , and TEC have been calculated. The magnitudes computed by the methods described earlier for both composites are of a high level and are comparable to those of the individual solid-solution constituents; the value of $RC(RCP)$ for composite 1 ($\mu_0\Delta H=1$ T) is equal to 57(67) J/kg and, for composite 2 ($\mu_0\Delta H=2$ T), it is 122(150) J/kg. The $TEC(3)$ values obtained for both composites are comparable to their maximum isothermal magnetic entropy change values, which result directly from the scope of ΔT_{lifft} values. In the case of $TEC(10)$, the values are slightly smaller in comparison with $TEC(3)$; however, they are still of a high level and comparable to those of the solid solution constituents (see Table 1).

Evaluation Of The Magnetocaloric Effect With Direct Measurements

The adiabatic temperature change ΔT_{ad} caused by the magnetic field change $\mu_0\Delta H$, i.e., the magnetocaloric effect, has been additionally determined by direct temperature measurements in the range of magnetic fields up to 14 T. Figures 6(a) and (b) show experimental ΔT_{ad} vs. the initial temperature, as obtained in the magnetizing process, for $\text{Ho}_{0.75}\text{Er}_{0.25}\text{Ni}_2$ and $\text{Ho}_{0.5}\text{Er}_{0.5}\text{Ni}_2$, respectively. The initial field was zero in all cases. As expected, the increase of the applied magnetic field leads to an increase in ΔT_{ad} . The maximum value of ΔT_{ad} at $\mu_0\Delta H=14$ T reaches 16.4 K at T_C for $\text{Ho}_{0.75}\text{Er}_{0.25}\text{Ni}_2$, and 15.1 K at T_C for $\text{Ho}_{0.5}\text{Er}_{0.5}\text{Ni}_2$. The maxima of ΔT_{ad} obtained at 1- and 2-T magnetic field changes by both direct and indirect methods have been detected at the same temperature and the determined values are in good agreement.

Table 2

Experimental data characterizing the adiabatic temperature change, ΔT_{ad} , due to MCE caused by the magnetic field change, $\mu_0\Delta H$, for the selected binary RNi₂ intermetallic compounds and for Ho_{0.75}Er_{0.25}Ni₂ and Ho_{0.5}Er_{0.5}Ni₂ solid solutions. A is the coefficient from equation $\Delta T_{ad} = A(\mu_0\Delta H)^{2/3}$. The data were obtained by direct measurements of ΔT_{ad} during the field change, $\mu_0\Delta H$, achieved by using the extraction method in a Bitter magnet. The values of ΔT_{ad} marked with ‡ symbol are estimated by the extrapolation of the $\Delta T_{ad} = A(\mu_0\Delta H)^{2/3}$ relation.

Compound	T_C (K)	ΔT_{ad} (K)						A (K/T ^{2/3})
		0–1 T	0–2 T	0–5 T	0–8 T	0–10 T	0–14 T	
TbNi ₂ [23]	37.1	1.5‡	2.4	4.6	6.2	6.9	8.4‡	1.45
DyNi ₂ [23]	21.8	2.3	3.6	7.1	9.2	10.6	13.4‡	2.31
HoNi ₂ [10]	13.5	2.8‡	4.2	8.7	11.4	12.9	16.3‡	2.8
Ho _{0.75} Er _{0.25} Ni ₂	12.0	2.9	5.1	9.6	12.7	13.9	16.3	2.9
Ho _{0.5} Er _{0.5} Ni ₂	9.7	2.6	4.5	8.3	11.2	12.9	15.1	2.6
ErNi ₂ [10]	6.2	2.1‡	3.5	6.2	8.8	9.8	12.2‡	2.1

Directly measured maximum ΔT_{ad} as a function of the final magnetic field is plotted in Figs. 6(c)-(d). For both Ho_{0.75}Er_{0.25}Ni₂ and Ho_{0.5}Er_{0.5}Ni₂ solid solutions, ΔT_{ad} grows nonlinearly with increasing $\mu_0\Delta H$. Characteristic quantity $\Delta T_{ad}/\mu_0\Delta H$ decreases from 2.8 K/T at 1 T to 1.2 K/T at 14 T for Ho_{0.75}Er_{0.25}Ni₂, and from 2.7 K/T at 1 T to 1.1 K/T at 14 T for Ho_{0.5}Er_{0.5}Ni₂.

To check the applicability of the thermodynamic Landau theory for the description of our experimental results, the adiabatic temperature change ΔT_{ad} was plotted as a function of $(\mu_0\Delta H)^{2/3}$, as shown in insets in Figs. 6(c)-(d). The linear behavior of the dependences for both investigated compounds near their Curie temperature demonstrates a good agreement between the experimental results and thermodynamic Landau theory.

By plotting the maximum ΔT_{ad} value versus $(\mu_0\Delta H)^{2/3}$ and using an equation: $\Delta T_{ad} = A(\mu_0\Delta H)^{2/3}$, where A is a characteristic parameter of magnetocaloric materials, one can obtain information about the magnetocaloric properties of investigated samples [30]. By fitting the experimental data, we find $A = 2.9$ K/T^{2/3} for Ho_{0.75}Er_{0.25}Ni₂ and $A = 2.6$ K/T^{2/3} for Ho_{0.5}Er_{0.5}Ni₂. These values are comparable with those obtained for the parent compounds and other binary Laves-phase compounds and are also comparable with the values of the most efficient magnetic refrigerants, such as Gd ($A = 3.83$ K/T^{2/3}) and LaFe_{11.2}Si_{1.8} ($A = 2.16$ K/T^{2/3}) [30]. The data obtained by direct measurements are gathered in Table 2.

Discussion

The present study, by an example of $\text{Ho}_{1-x}\text{Er}_x\text{Ni}_2$, develops the concept of magnetocaloric efficiency of the rare-earth Laves-phase solutions starting from their magneto thermodynamic properties and then proceeds illustrating their potentiality as components of magnetocaloric composites.

The analysis of the structural data obtained for the $\text{Ho}_{1-x}\text{Er}_x\text{Ni}_2$ solid solutions confirms the similarity of the structures of the parent HoNi_2 and ErNi_2 binary compounds and the Ho diluted compound with $x = 0.25$, which have the regular C15 cubic structure (Laves phase). The subsequent introduction of Ho to $x = 0.5$ and 0.75 leads to the formation of a cubic superstructure that is due to a regular arrangement of vacancies at rare earth sites and decreases the crystal lattice symmetry (space group $F43m$). The superstructure is characterized by the doubled lattice parameter.

The measurements of the heat capacity were performed for the compounds, the phase and chemical compositions of which were well characterized. The data demonstrate that the substitution of Ho atoms for Er atoms markedly modifies the magnetic behavior of the $\text{Ho}_{1-x}\text{Er}_x\text{Ni}_2$ system. The appearance of Er atoms in the rare-earth sublattice results in the common magnetic dilution consisted in weakening the exchange interactions, which is accompanied by the decrease in the ordering temperature. Thus, its linear variations, namely, decrease in the Curie temperature of the system from 12.0 K (for $\text{Ho}_{0.75}\text{Er}_{0.25}\text{Ni}_2$) to 7.7 K (for $\text{Ho}_{0.25}\text{Er}_{0.75}\text{Ni}_2$) are realized by the mutual substitutions of rare-earth components.

The magnetothermodynamics properties of the three-component solid solutions were characterized by indirect evaluation and direct measurements of magnetocaloric potentials in a wide range of magnetic fields. The possibility of precise tailoring the magnetocaloric potentials to a certain temperature range was demonstrated. As the Er content increases, the maximum magnetic entropy change decreases from 16.2 J/kgK for $\text{Ho}_{0.75}\text{Er}_{0.25}\text{Ni}_2$ at 12 K and reaches 13.7 J/kgK at 7.7 K for $\text{Ho}_{0.25}\text{Er}_{0.75}\text{Ni}_2$ for a magnetic field change of 2 T. The maximum adiabatic temperature change ΔT_{ad} for $\text{Ho}_{0.75}\text{Er}_{0.25}\text{Ni}_2$ in the 2-T magnetic field change is equal to 4.9 K at 12 K, and with increasing Er content, the ΔT_{ad} value decreases to 3.9 K for $\text{Ho}_{0.25}\text{Er}_{0.75}\text{Ni}_2$ in the vicinity of T_C . The maximum values of the adiabatic temperature change, determined by the direct measurements, reach 16.4 K near 12.0 K for $\text{Ho}_{0.75}\text{Er}_{0.25}\text{Ni}_2$ and 15.1 K near 9.7 K for $\text{Ho}_{0.5}\text{Er}_{0.5}\text{Ni}_2$ at $\mu_0\Delta H = 14$ T. The maximum values of ΔT_{ad} , obtained at 1- and 2-magnetic fields, obtained by direct and indirect methods are in good agreement. The directly measured adiabatic temperature changes near the Curie temperature in high magnetic fields were compared with the values obtained based on the Landau theory for the second-order phase transitions. It was demonstrated that, the magnetic field dependence of ΔT_{ad} obeys the $(\mu_0\Delta H)^{2/3}$ function with the parameter A , which characterizes intrinsic properties of refrigerants.

Additionally, the availability of the magnetocaloric potentials experimentally estimated for the individual three-component $\text{Ho}_{1-x}\text{Er}_x\text{Ni}_2$ solid solutions allows us to simulate optimal molar ratios to construct the composites to be considered as a refrigerant material in magnetic refrigerators performing an Ericsson

cycle at low temperatures. These theoretical results based on the real empirical data are very optimistic and are of interest to perform further experimental studies. The results of the simulation indicate that the proposed composite exhibits a high potential for the application in magnetic refrigeration devices, especially in the cryogenic temperature range.

Methods

Sample preparation, structural analysis, heat capacity, and direct magnetocaloric measurements

$\text{Ho}_{1-x}\text{Er}_x\text{Ni}_2$ alloys with $x = 0.25, 0.5, \text{ and } 0.75$ were prepared by repeated arc-melting of appropriate amounts of starting metals in a high-purity argon atmosphere at a pressure of 1.5 atm; starting metallic components of at least 99. % (rare-earths) and 99.9 % (Ni) purity were used. The obtained ingots were wrapped separately with Mo foil and subsequently subjected to homogenizing annealing in an argon-filled quartz tube. The annealing process was performed at 1123 K for one month; subsequently, the ingots were subjected to slow furnace cooling to room temperature to ensure their uniform cooling, exclude the fixation of high-temperature structural state of compounds, and to obtain their equilibrium state. The elemental composition was assessed by energy dispersive X-ray (EDX) spectroscopy with the simultaneous study of the sample's microstructure by scanning electron microscopy (SEM) using an FEI Nova Nano SEM 230 scanning electron microscope (operating at an accelerating voltage of 20 kV) equipped with an energy-dispersive spectrometer (EDAX Genesis XM4). The crystal structure was determined by X-ray diffraction (XRD) analysis, which was carried out at room temperature using powdered samples and an Ultima IV Rigaku (Japan) diffractometer equipped with a "D/teX" high-speed semiconductor detector. X-ray diffraction patterns were taken in an angular range of $9\text{-}100^\circ$ at a step of 0.02° using $\text{CuK}\alpha$ radiation and a fluorescent correction regime.

Heat capacity was measured in the 2–100 K temperature range in zero, 1- and 2-T magnetic fields by a relaxation method using a PPMS-14 installation (Quantum Design, USA). The direct measurements of ΔT_{ad} were performed in the 4.2–50 K temperature range in magnetic fields up to 14 T using the original setup, which is based on the extraction method and allows us to perform direct measurements of the adiabatic temperature change [31]. Steady magnetic fields up to 14 T were generated by a Bitter-type magnet, and a maximum field-change rate of $\sim 6 \text{ T/s}$ was obtained by moving the sample in and out of the applied magnetic field.

Declarations

Acknowledgements

The work was supported by the National Science Center, Poland through the OPUS Program under Grant No. 2019/33/B/ST5/01853.

References

1. Pecharsky, V. K. & Gschneidner Jr, K. A. Magnetocaloric effect and magnetic refrigeration. *J. Magn. Mater.* **200**, 44–56 (1999).
2. Tishin, A. M. & Spichkin, Y. I. Recent progress in magnetocaloric effect: Mechanisms and potential applications. *Int. J. Refrigeration* **37**, 223–229 (2014).
3. Kitanovski, A. et al. *Magnetocaloric Energy Conversion, From Theory to Applications*, Springer International Publishing Switzerland (2015).
4. Griffith, L. D., Mudryk, Y., Slaughter, J. & Pecharsky, V. K. Material-based figure of merit for caloric materials. *J. Appl. Phys.* **123**, 034902 (2018).
5. Delsante, S., Stifanese, R. & Borzone, G. Thermodynamic stability of RNi_2 Laves phases. *J. Chem. Thermodynamics*. **65**, 73–77 (2013).
6. Kirchmayr, H. R. & Burzo, E. in: H. P. J. Wijn (Ed.), *Landolt–Börnstein, New Series III/19d2*, Berlin, (1990).
7. Latroche, M., Paul-Boncour, V. & Percheron-Guegan, A. Structural Instability in $R_{1-x}Ni_2$ Compounds and Their Hydrides (R = Y, Rare Earth). *Z. Phys. Chem.* **179**, 261–268 (1993).
8. Gratz, E. et al. Temperature- and pressure-induced structural transitions in rare-earth-deficient (R = Y, Sm, Gd, Tb) Laves phases. *J. Phys. Condens. Matter* **8**, 8351 (1996).
9. Wallace, W. E. & Segal, E. in: A.M. Alper, J.L. Margrave, A.S. Nowick (Eds.), *Rare Earth Intermetallics*, Academic Press, New York, (1973).
10. Ówik, J., Koshkid'ko, Y., Nenkov, K., Tereshina, E. A. & Rogacki, K. Structural, magnetic and magnetocaloric properties of $HoNi_2$ and $ErNi_2$ compounds ordered at low temperatures. *J. Alloys Compd.* **735**, 1088–1095 (2018).
11. Hashimoto, T. et al. New application of complex magnetic materials to the magnetic refrigerant in an Ericsson magnetic refrigerator. *J. Appl. Phys.* **62**, 3873 (1987).
12. Ówik, J. et al. Magnetocaloric prospects of mutual substitutions of rare-earth elements in pseudobinary $Tb_{1-x}Ho_xNi_2$ compositions ($x = 0.25-0.75$). *J. Alloys Compd.* **886**, 161295 (2021).
13. Ówik, J., Koshkid'ko, Y., de Oliveira, N. A., Mikhailova, A. & Nenkov, K. Effect of composition changes on the structural, magnetic and thermodynamic properties in $Tb_{1-x}Dy_xNi_2$ intermetallic compounds. *J. Alloys Compd.* **769**, 588–596 (2018).
14. Ówik, J. et al. Experimental and theoretical analysis of magnetocaloric behavior of $Dy_{1-x}Er_xNi_2$ intermetallics ($x = 0.25, 0.5, 0.75$) and their composites for low-temperature refrigerators performing an Ericsson cycle. *Phys. Rev. B* **103**, 214429 (2021).
15. Lea, K. R., Leask, M. J. M. & Wolf. W. P. The raising of angular momentum degeneracy of f-Electron terms by cubic crystal fields. *J. Phys. Chem. Solids* **23**, 1381–1405 (1962).
16. Ówik, J. et al. Magnetic properties and specific heat of $Dy_{1-x}La_xNi_2$ compounds. *J. Magn. Mater.* **321**, 2821–2826 (2009).
17. Gschneidner, K. A., Pecharsky, V. K., Gailloux. M. J. & Takeya, H. Utilization of the magnetic entropy in active magnetic regenerator materials, *Adv. Cryog. Eng.* **42**, 465–474 (1996).

18. Gschneidner Jr, K. A. *et al.* Recent Developments in Magnetic Refrigeration. Mater. Sci. Forum **315–317**, 69–76 (1999).
19. Franco, V. *et al.* Magnetocaloric effect: From materials research to refrigeration devices. Prog. Mater. Sci. **93**, 112–232 (2018).
20. Gorria, P. *et al.* Relative cooling power enhancement in magneto-caloric nanostructured Pr₂Fe₁₇. J. Phys. D: Appl. Phys. **41**, 192003 (2008).
21. Griffith, L. D., Mudryk, Y., Slaughter, J. & Pecharsky, V. K. Material-based figure of merit for caloric materials. J. Appl. Phys. **123**, 034902 (2018).
22. Sánchez Llamazares, J. L. *et al.* Magnetic entropy change and refrigerant capacity of rapidly solidified TbNi₂ alloy ribbons. J. Appl. Phys. **113**, 17A912 (2013).
23. Ówik, J. *et al.* Magnetocaloric effect in Laves-phase rare-earth compounds with the second-order magnetic phase transition: Estimation of the high-field properties. Acta Mater. **133**, 230–239 (2017).
24. von Ranke, P. J., Pecharsky, V. K. & Gschneidner Jr, K. A. Influence of the crystalline electrical field on the magnetocaloric effect of DyAl₂, ErAl₂, and DyNi₂. Phys. Rev. B. **58**, 12110 (1998).
25. Mo, Z. J. *et al.* Magnetic property and magnetocaloric effect in TmCoAl compound. Intermetallics **56**, 75–78 (2015).
26. Samanta, T., Das, I. & Banerjee, S. Giant magnetocaloric effect in antiferromagnetic ErRu₂Si₂ compound. Appl. Phys. Lett. **91**, 152506 (2007).
27. Li, L. *et al.* Large Magnetic Entropy Change in Dy_{1-x}Ho_xNi₂B₂C (x = 0–1) Superconductors. Appl. Phys. Exp. **4**, 093101 (2011).
28. Hashimoto, T. *et al.* A new method of producing the magnetic refrigerant suitable for the Ericsson magnetic refrigeration. IEEE Trans. Magn. **23**, 2847–2849 (1987).
29. Smaili, A. & Chahine, R. Composite Magnetic Refrigerants for an Ericsson Cycle: New Method of Selection Using a Numerical Approach Adv. Cryog. Eng. **42**, 445–450 (1996).
30. Kuz'min, M. D. *et al.* Magnetic field dependence of the maximum adiabatic temperature change. Appl. Phys. Lett. **99**, 012501 (2011).
31. Koshkid'ko, Y. *et al.* Magnetocaloric properties of Gd in fields up to 14 T. J. Magn. Magn. Mater. **433**, 234–238 (2017).

Figures

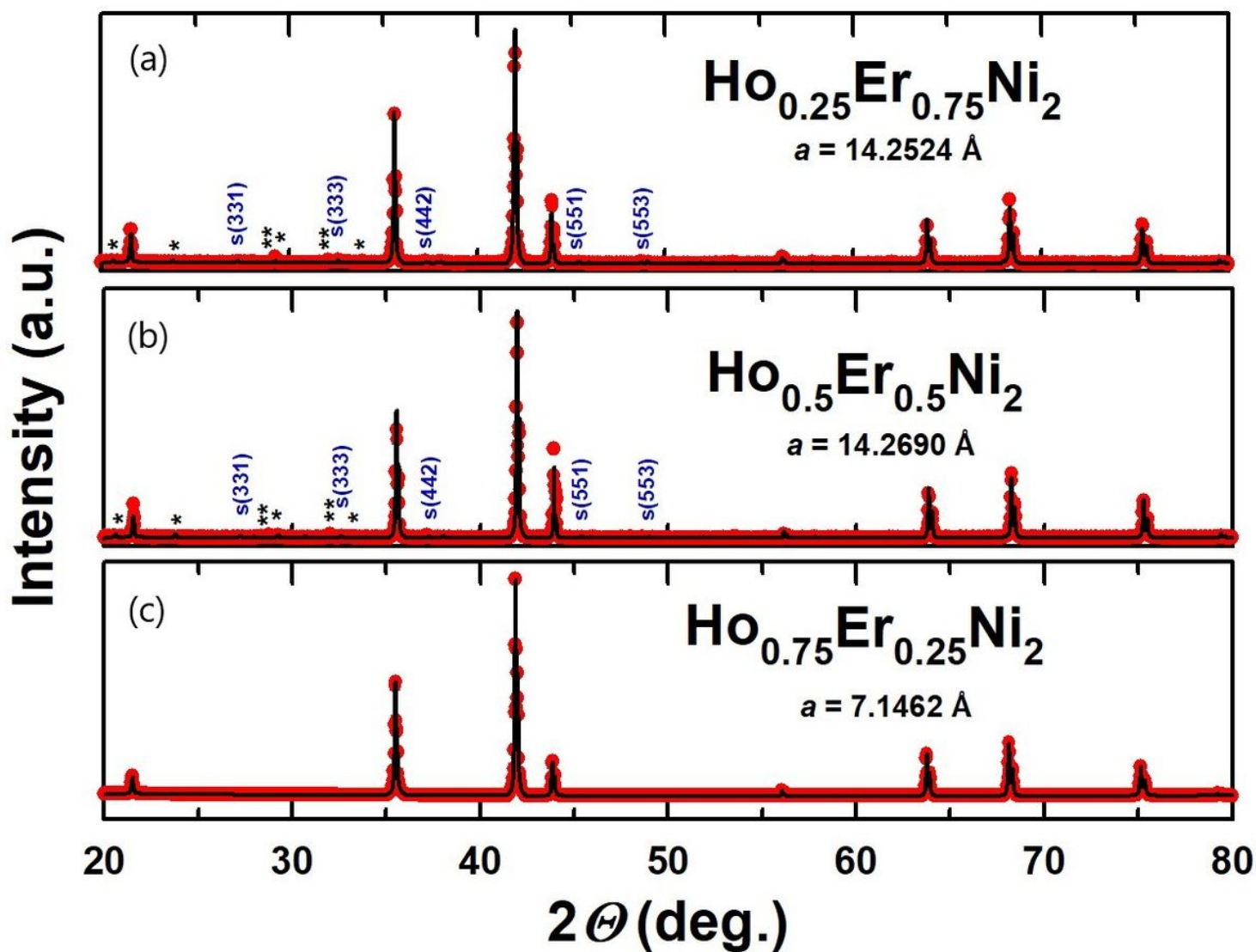


Figure 1

Results of the Rietveld refinement of the room-temperature XRD patterns taken for $\text{Ho}_{0.25}\text{Er}_{0.75}\text{Ni}_2$ (a), $\text{Ho}_{0.5}\text{Er}_{0.5}\text{Ni}_2$ (b) and $\text{Ho}_{0.75}\text{Er}_{0.25}\text{Ni}_2$ (c). Peaks marked with S correspond to the superstructure (F-43m space group) and peaks for the rare-earth (Ho,Er) $_2\text{O}_3$ oxide phases are marked with * and **.

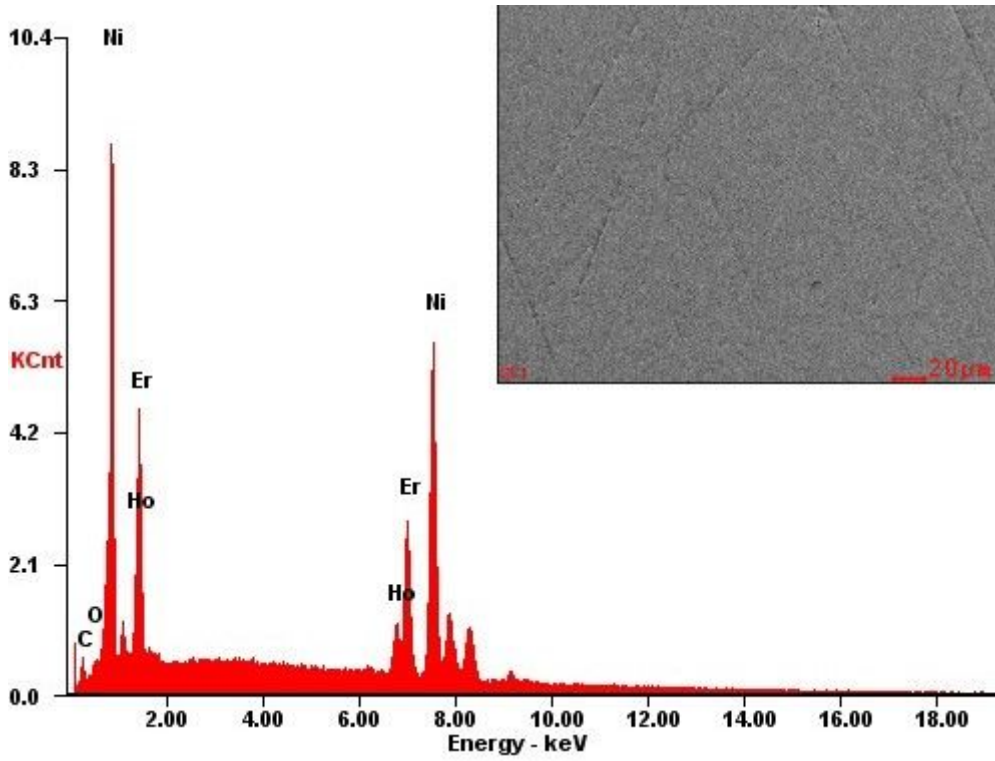


Figure 2

Energy-dispersive x-ray (EDX) analysis data for the Ho_{0.25}Er_{0.75}Ni₂ solid solution and SEM image (with secondary electrons contrast) of the typical polished surface.

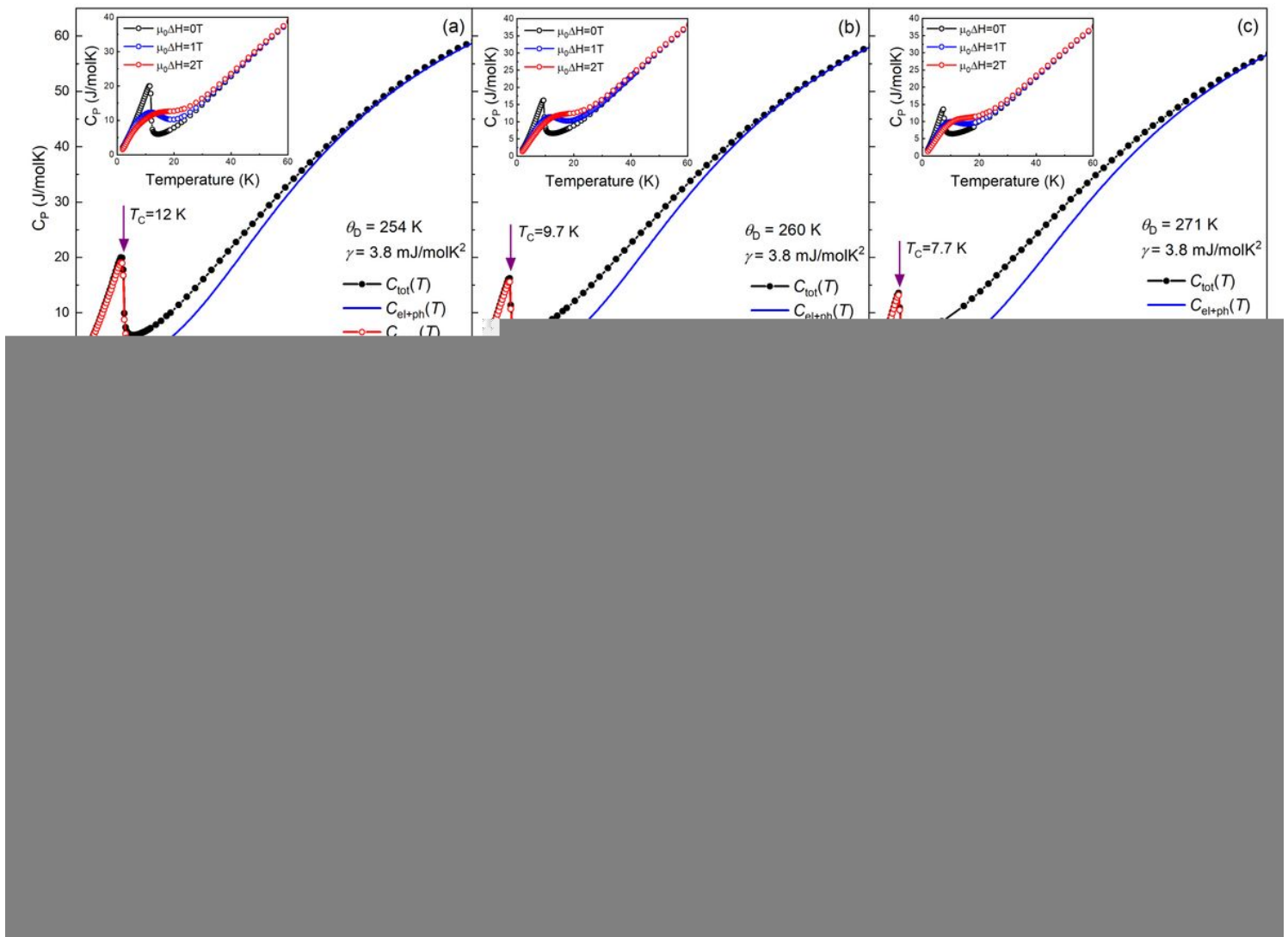


Figure 3

Total heat capacity $C_{\text{tot}}(T)$ of $\text{Ho}_{0.75}\text{Er}_{0.25}\text{Ni}_2$ (a), $\text{Ho}_{0.5}\text{Er}_{0.5}\text{Ni}_2$ (b) and $\text{Ho}_{0.25}\text{Er}_{0.75}\text{Ni}_2$ (c) measured in zero magnetic field. The calculated sum of electronic and phonon contributions $C_{\text{el+ph}}$ as well as estimated magnetic contribution C_{mag} . The insets of (a)-(c) show the heat capacity as a function of temperature measured in zero, 1- and 2-T magnetic fields, respectively. Temperature dependences of the magnetic entropy $S_{\text{mag}}(T)$ for $\text{Ho}_{0.75}\text{Er}_{0.25}\text{Ni}_2$ (d), $\text{Ho}_{0.5}\text{Er}_{0.5}\text{Ni}_2$ (e) and $\text{Ho}_{0.25}\text{Er}_{0.75}\text{Ni}_2$ (f) in zero, 1- and 2-T magnetic fields. The horizontal dotted lines correspond to the theoretical maximum value $S_{\text{max}} = R \ln(2J + 1)$ and the vertical dotted lines correspond to the magnetic phase transition temperature T_C . Insets show the magnetic entropy change ΔS_{mag} measured for magnetic field changes of 1 and 2 T.

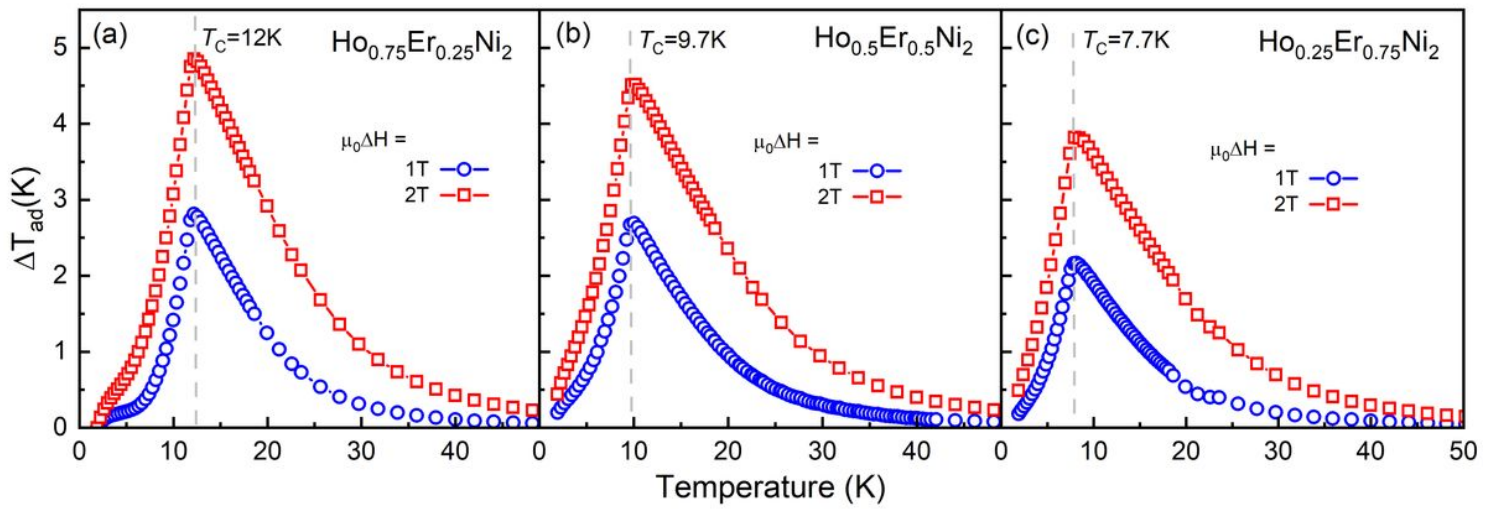


Figure 4

Temperature dependences of the adiabatic temperature change, ΔT_{ad} , of $\text{Ho}_{0.75}\text{Er}_{0.25}\text{Ni}_2$ (a), $\text{Ho}_{0.5}\text{Er}_{0.5}\text{Ni}_2$ (b) and $\text{Ho}_{0.25}\text{Er}_{0.75}\text{Ni}_2$ (c) calculated from heat capacity data measured in 1- and 2-T magnetic fields.

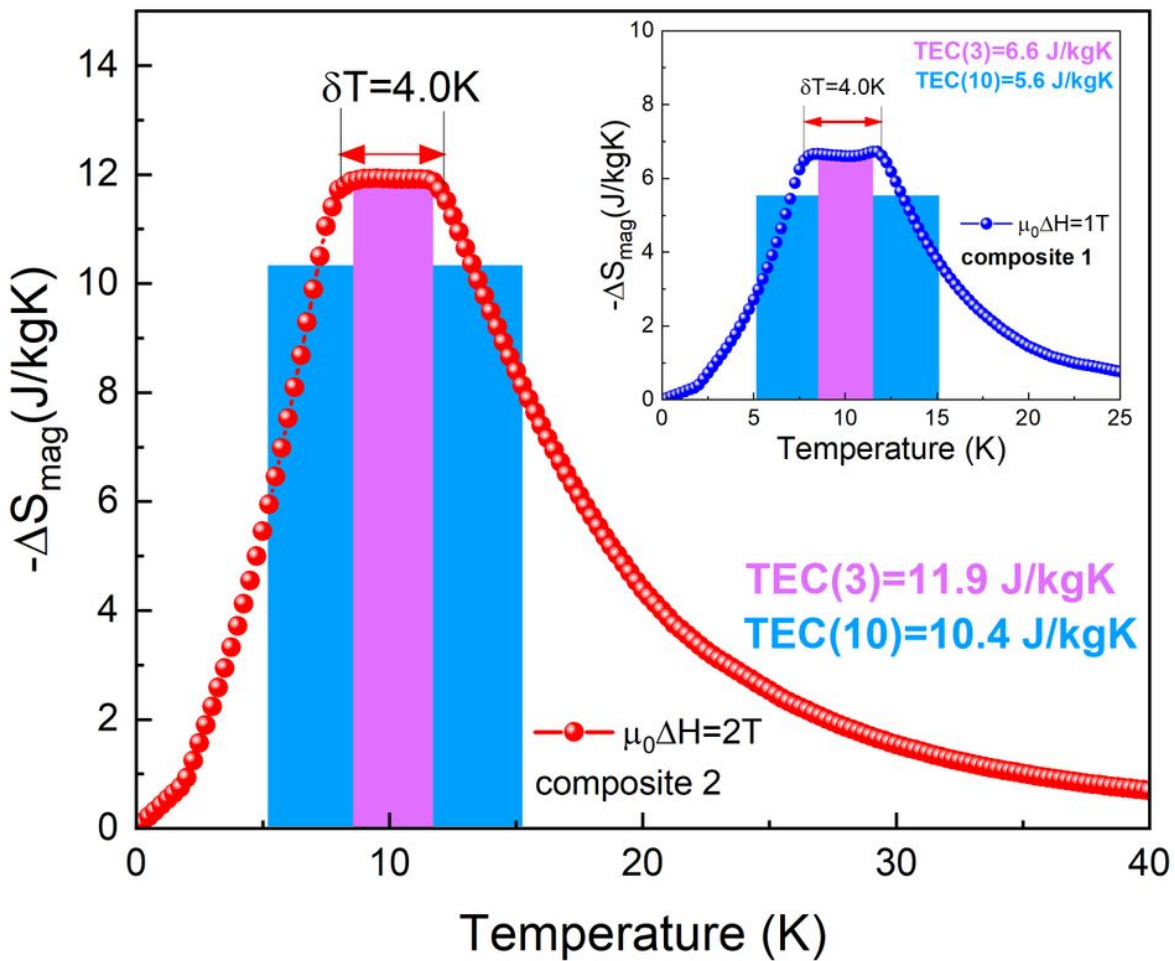


Figure 5

Temperature dependences of the isothermal magnetic entropy change $-\Delta S_{\text{mag}}(T)$ and temperature averaged entropy change $\text{TEC}(3)$ and $\text{TEC}(10)$ calculated for composites based on the investigated compounds, for magnetic field changes of 1 T (inset) and 2 T.

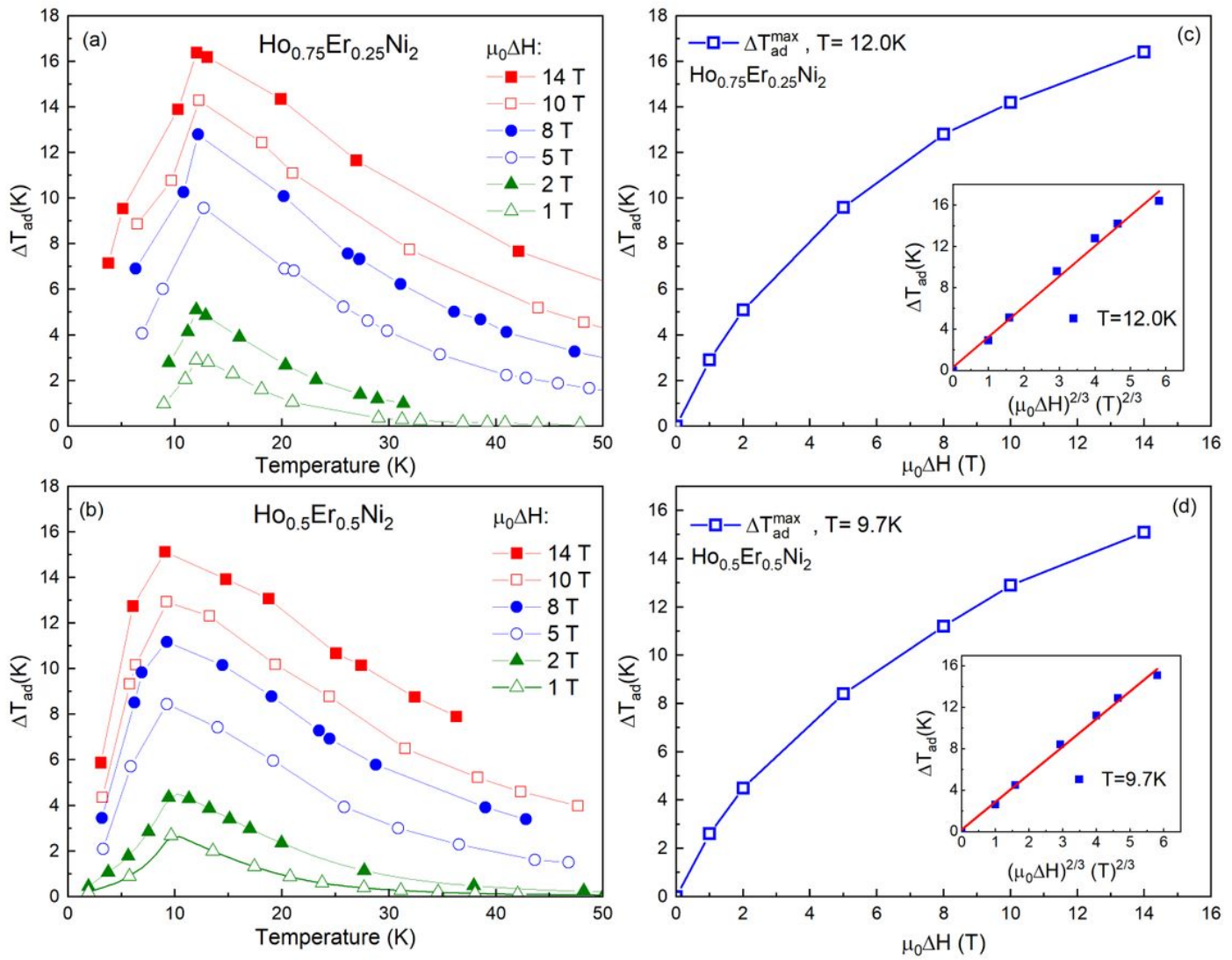


Figure 6

Temperature dependences of the adiabatic temperature change, ΔT_{ad} , obtained by direct measurements for $\text{Ho}_{0.75}\text{Er}_{0.25}\text{Ni}_2$ (a) and $\text{Ho}_{0.5}\text{Er}_{0.5}\text{Ni}_2$ (b) at different magnetic field changes $\mu_0\Delta H$ and maximum adiabatic temperature change, ΔT_{ad}^{\max} , for $\text{Ho}_{0.75}\text{Er}_{0.25}\text{Ni}_2$ (c), $\text{Ho}_{0.5}\text{Er}_{0.5}\text{Ni}_2$ (d) as a function of the magnetic field change, $\mu_0\Delta H$. Insets show the ΔT_{ad} as a function of $(\mu_0\Delta H)^{2/3}$. Solid lines present the relation $\Delta T_{ad} = A(\mu_0\Delta H)^{2/3}$, with A listed in Table 2.